J|A|C|S ARTICLES

Published on Web 04/06/2010

$Fe_xPb_{4-x}Sb_4Se_{10}$: A New Class of Ferromagnetic Semiconductors with Quasi 1D $\{Fe_2Se_{10}\}$ Ladders

Pierre F. P. Poudeu,* Nathan Takas, Clarence Anglin, James Eastwood, and Arianna Rivera

The Advanced Materials Research Institute and Department of Chemistry, University of New Orleans, New Orleans, Louisiana 70148

Received December 14, 2009; E-mail: ppoudeup@uno.edu

Abstract: A new family of quasi-one-dimensional ferromagnetic selenides with general formula $Fe_xPb_{4-x}Sb_4Se_{10}$ ($0 \le x \le 2$) was generated by isoelectronic substitution in octahedral positions of Pb atoms by Fe within the structure of $Pb_4Sb_4Se_{10}$. Two members of this family with $x = 0.75$ and $x = 1$ were synthesized as a single phase through direct combination of the elements at 823 K. Single crystal X-ray diffraction revealed that $Fe_{0.75}Pb_{3.25}Sb_4Se_{10}$ crystallizes with the orthorhombic space group *Pnma*, whereas $Fe_{0.96}Pb_{3.04}Sb_4Se_{10}$ adopts the lower symmetry monoclinic subgroup $P2(1)/m$ (#11). Both compounds are isomorphous with $Pb_4Sb_4Se_{10}$, and their crystal structures consist of corrugated layers of edge-sharing bicapped trigonal prisms and octahedra around Pb atoms. Adjacent layers are interconnected by NaCl-type {SbSe} ribbons. The voids left by this arrangement are filled by the novel one-dimensional $\{Fe_2Se_{10}\}$ double chains (ladder) of edge-sharing octahedra running along [010]. Temperature dependent magnetic susceptibility as well as field dependent magnetization isotherms showed that both $Fe_{0.75}Pb_{3.25}Sb_4Se_{10}$ and $FePb_3Sb_4Se_{10}$ are ferromagnetic below 300 K and exhibit superparamagnetism at higher temperatures. A dramatic reduction in the magnetic moment per Fe^{2+}, $\sim$0.40 μ_B, was observed in $Fe_{0.75}Pb_{3.25}Sb_4Se_{10}$ and $FePb_3Sb_4Se_{10}$ suggesting that the $Fe_xPb_{4-x}Sb_4Se_{10}$ ($0 \le x \le 2$) phases are not ordinary ferromagnets where all the magnetic spins are parallel at low temperatures. Analysis of the magnetic coupling of spins located on adjacent Fe atoms (within a localized Fe^{2+} moment picture) using Goodenough−Kanamori rules suggested that the magnetism within the ladder and ladder-single chain systems in $Fe_xPb_{4-x}Sb_4Se_{10}$ phases is controlled by competing interactions.

Introduction

Impressive advances in the chemistry of multinary metal chalcogenides have been made over the past decades through the investigation of both synthetic and natural phases.[1−6] The renewed interest in this family of compounds has been motivated by the tremendous variety of physical properties such as thermoelectrics,[7−9] nonlinear optics,[10] photoelectronics,[11] and solid-state electrolytes[12−14] that can result from the diversity and flexibility of their framework structures. Despite the considerable number of ternary and quaternary metal chalcogenides reported so far, very little effort has been made to take advantage of their composition and structural flexibility so as to design new materials with multiple functionalities. For example, the low symmetry associated with known ternary semiconducting phases such as $Pb_4Sb_4Se_{10}$,[15] $Pb_4Sb_6Se_{13}$,[16] and $Pb_6Sb_6Se_{17}$[16] can be exploited to target new low-dimensional magnetic semiconductors by selective substitution of some Pb atoms in octahedral positions with magnetic transition metal elements, e.g. Mn and Fe. Such compounds are interesting not only because they provide an excellent platform for the investigation of interactions between magnetic ions, charge carriers, orbital degrees of freedom, and their coupling with the crystal lattice but also because they can play key roles in the development of new types of molecular-scale high density data storage and nonvolatile fast memory.[17]

Over the past decades, there have been growing numbers of purely inorganic compounds in which low-dimensional magnetic

(1) Mrotzek, A.; Kanatzidis, M. G. *Acc. Chem. Res.* **2003**, *36*, 111–119.
(2) Kanatzidis, M. G.; Sutorik, A. C. *Prog. Inorg. Chem.* **1995**, *43*, 151–265.
(3) Eichhorn, B. W. *Prog. Inorg. Chem.* **1994**, *42*, 139–237.
(4) Kanatzidis, M. G. *Acc. Chem. Res.* **2005**, *38*, 359–368.
(5) Makovicky, E. *Eur. J. Mineral* **1993**, *5*, 545–591.
(6) Makovicky, E. *Rev. Mineral. Geochem.* **2006**, *6*, 7–125.
(7) Rowe, D. M., Ed. *CRC Handbook of Thermoelectrics*; CRC Press: Boca Raton, FL, 1995.
(8) Kanatzidis, M. G. *Semicond. Semimet.* **2001**, *69*, 51–100.
(9) Chung, D. Y.; Hogan, T.; Brazis, P.; Rocci-Lane, M.; Kannewurf, C.; Bastea, M.; Uher, C.; Kanatzidis, M. G. *Science* **2000**, *287*, 1024–1027.
(10) Ballman, A. A.; Byer, R. L.; Eimerl, D.; Feigelson, R. S.; Feldman, B. J.; Goldberg, L. S.; Menyuk, N.; Tang, C. L. *Appl. Opt.* **1987**, *26*, 224–227.
(11) Ibuki, S.; Yoshimatsu, S. *J. Phys. Soc. Jpn.* **1955**, *10*, 549–554.
(12) Shionoya, S.,Yen, W. M., Eds. *Phosphor Handbook*; CRC Press: Boca Raton, FL, 1999.
(13) Matsushita, Y.; Kanatzidis, M. G. *Z. Naturforsch.* **1998**, *B53*, 23–30.
(14) Kanno, R.; Hata, T.; Kawamoto, Y.; Irie, M. *Solid State Ionics* **2000**, *130*, 97–104.
(15) Showron, A.; Brown, I. D. *Acta Crystallogr.* **1990**, *C46*, 2287–2291.
(16) Derakhshan, S.; Assoud, A.; Taylor, N. J.; Kleinke, H. *Intermetallics* **2005**, *14*, 198–207.
(17) Rocha, A.; Garcia-Suarez, V.; Bailey, S.; Lambert, C.; Ferrer, J.; Sanvito, S. *Nat. Mater.* **2005**, *4*, 335.

phenomena are reported. Some examples are $CuGeO_3$[18] in which a spin-Peierls transition was observed, the Haldame compounds Y_2NiBaO_5[19] and $FePb_4Sb_6S_{14}$[20] which show 1D-Heisenberg antiferromagnetic behavior, and, much more recently, the $KNaMSi_4O_{10}$ (M = Cu, Mn, Fe)[21] phases in which the magnetic behavior within the one-dimensional M_2O_8 dimeric units follow the Heisenberg−Dirac−van Vleck Hamiltonian. In purely inorganic low-dimensional magnetic compounds, the inorganic framework separating magnetic domains plays the role of the organic ligands which help to preserve the low-dimensional character in organometallic molecular magnets.[22] The indirect exchange or superexchange interactions that govern the magnetic behavior in such low-dimensional magnetic inorganic compounds can be qualitatively understood using occupied orbitals, bond lengths, and angles through the Goodenough−Kanamori rules.[23−25] However, the sign and magnitude of the magnetic interactions can be influenced by other factors such as the nature of the bridging anionic atoms (covalency of the bond), the distortion of the local environment of the magnetic atoms, and the structural and chemical parameters of the inorganic framework separating magnetic domains in the structure.[26,27] For low-dimensional magnetic systems with metal chalcogenide frameworks such as the minerals Jamesonite ($FePb_4Sb_6S_{14}$)[20,28] and Benavidesite ($MnPb_4Sb_6S_{14}$)[28] in which 1D infinite $\{(Fe/Mn)S_6\}$ single magnetic chain was reported, the strength of Sb−S and Pb−S covalent bonds in the rigid $\{Pb_4Sb_6S_{13}\}$ framework can significantly shape the geometry of the $[MS_6]$ octahedral coordination and therefore also affect the type and magnitude of the superexchange interaction of two spins on adjacent transition metal centers.[20,23,24]

In this work, a new family of low-dimensional magnetic semiconductors with general composition $Fe_xPb_{4-x}Sb_4Se_{10}$ ($0 \le x \le 2$) was rationally designed from the structure of $Pb_4Sb_4Se_{10}$,[15] the selenium analogue of the mineral cosalite, through substitution of Pb atoms by Fe atoms in octahedral positions. The $Pb_4Sb_4Se_{10}$ structure was selected as a template for the search for low-dimensional magnetic semiconductors because it presents interesting features such as the geometry of octahedra around Pb atoms as well as their connectivity with the remaining 3D structure. Preliminary analysis of the geometry of octahedra around Pb atoms in the structure of $Pb_4Sb_4Se_{10}$ revealed distortion from regular octahedral coordination toward [2 + 4] geometry with two short apical bonds and four long equatorial bonds. This type of distortion is similar to that of $\{MS_6\}$ (M = Fe, Mn) octahedra in the single magnetic chain compounds $MPb_4S_6S_{14}$ (M = Mn, Fe),[20,28] MSb_2S_4 (M = Mn, Fe),[29] and $Tl_2MnAs_2S_5$.[30] This suggested that transition metal atoms such as Fe and Mn will preferentially substitute Pb atoms in octahedral positions when attempting to form isostructural quaternary compounds through substitution of some Pb atoms in the structure of $Pb_4Sb_4Se_{10}$. Although according to Goldschmidt's substitution rules,[31] the large difference in effective ionic radii (ΔR) of Fe^{2+} (high spin, 0.78 Å; low spin, 0.61 Å) and Pb^{2+} (1.19 Å) in octahedral coordination[32,33] and the difference in the electronegativity of Fe and Pb suggest little to no substitution between both elements, the natural occurrence of the $MPb_4Sb_6S_{14}$ (M = Mn, Fe) phases in which Fe^{2+} and Pb^{2+} coexist, strongly indicated that quaternary compounds containing a transition metal with the general formula $M_xPb_{4-x}Sb_4Se_{10}$ (M = Mn, Fe, etc.) are possible. In this paper, we show that despite the severe departure from the longstanding Goldschmidt's substitution rules, Fe^{2+} ions readily substitute Pb^{2+} ions in octahedral positions within the structure of $Pb_4Sb_4Se_{10}$ to generate a new family of ferromagnetic selenides with the general composition $Fe_xPb_{4-x}Sb_4Se_{10}$ ($0 \le x \le 2$), containing a novel quasi-one-dimensional $\{Fe_2Se_{10}\}$ dimeric chains (ladders). The crystal structures as well as magnetic and transport properties of $Fe_{0.75}Pb_{3.25}Sb_4Se_{10}$ and $FePb_3Sb_4Se_{10}$, two members of the $Fe_xPb_{4-x}Sb_4Se_{10}$ family, are reported. Analysis of structural details between $Fe_{0.75}Pb_{3.25}Sb_4Se_{10}$, $FePb_3Sb_4Se_{10}$, and $Pb_4Sb_4Se_{10}$ is used to understand the formation of the one-dimensional $\{Fe_2Se_{10}\}$ ladder and its impact on the observed magnetic properties.

Experimental Procedure

Synthesis. Single phases of $Fe_{0.75}Pb_{3.25}Sb_4Se_{10}$ and $FePb_3Sb_4Se_{10}$ were obtained from solid-state reactions involving elemental Fe (99.999%), Pb (99.99%), Sb (99.999%), and Se (99.999%). All reagents were purchased from Cerac and used as obtained. All four components in their powder form, weighed in the desired ratio under ambient atmosphere (total mass =10 g), were ground with an agate mortar and pestle and transferred into a fused silica tube ($\varnothing_{ID} = 9$ mm, Length =18 cm) which was flame-sealed under a residual pressure of $\sim 10^{-4}$ Torr. The sealed tube was placed into a tube furnace and heated stepwise to the target temperature 823 K at which a dwelling time of 72 h was imposed. The furnace was then slowly cooled to room temperature over 24 h. The resulting products were polycrystalline dark gray powders containing tiny needle-like single crystals. Alternatively, a single phase of $FePb_3Sb_4Se_{10}$ was obtained using the same reaction procedure, by combining binary FeSe and elemental Pb, Sb, and Se. Single crystals of $Fe_{0.75}Pb_{3.25}Sb_4Se_{10}$ and $FePb_3Sb_4Se_{10}$ suitable for X-ray single crystal structure determination were grown by annealing in a slight temperature gradient approximately 3 g of the synthesized polycrystalline powders sealed in a quartz tube under a residual pressure of 10^{-4} Torr. The temperature at the sample position was 823 K while the temperature at the other end was maintained at 873 K. Single crystals of $Fe_{0.75}Pb_{3.25}Sb_4Se_{10}$ and $FePb_3Sb_4Se_{10}$ were obtained at the initial sample position.

Specimens for electronic charge transport (electrical conductivity and thermopower) measurements were fabricated by hot pressing finely ground powders of $FePb_3Sb_4Se_{10}$ using a 10-ton uniaxial hot press system from Thermal Technologies Inc. The pressing was carried out under a dynamic vacuum of $\sim 10^{-4}$ Torr. An approximately 95% dense pellet (with a thickness of 2.4 mm and diameter of 13 mm) of $FePb_3Sb_4Se_{10}$ was obtained by applying a maximum pressure of 100 MPa with the furnace temperature set at 698 K. A rectangular bar specimen with dimensions 2.4 mm × 2.6 mm × 11 mm for simultaneous measurement of the electrical

(18) Hase, M.; Terasaki, I.; Uchinokura, K. *Phys. Rev. Lett.* **1993**, *70*, 3651.
(19) Ditusa, J. F.; Cheong, S. W.; Park, J. H.; Aeppli, G.; Broholm, G.; Chen, C. T. *Phys. Rev. Lett.* **1994**, *73*, 1857.
(20) Matsushita, Y.; Ueda, Y. *Inorg. Chem.* **2003**, *42*, 7830–7838.
(21) Brandao, P.; Rocha, J.; Reis, M. S.; dos Santos, A. M.; Jin, R. *J. Solid State Chem.* **2009**, *182*, 253–258.
(22) Verdaguer, M. *Polyhedron* **2001**, *20*, 1115.
(23) Goodenough, J. *J. Phys. Chem. Solids* **1958**, *6*, 287–297.
(24) Goodenough, J. *Phys. Rev.* **1955**, *100*, 564–573.
(25) Kanamori, J. *J. Phys. Chem. Solids* **1959**, *10*, 87–98.
(26) Hay, P.; Thibeault, J.; Hoffmann, R. *J. Am. Chem. Soc.* **1975**, *97*, 4884.
(27) Glerup, J.; Patricia, A.; Derek, J.; Kirsten, M. *Inorg. Chem.* **1995**, *34*, 6255.
(28) Leone, P.; Le Leuch, L.-M.; Palvadeau, P.; Molinie, P.; Moelo, Y. *Solid State Sci.* **2003**, *5*, 771–776.
(29) Buerger, M. J.; Hahn, T. *Am. Mineral.* **1955**, *40*, 226.
(30) Lukaszewicz, K.; Pietraszko, A.; Stepien-Damm, J.; Kajokas, A.; Grigas, J.; Drulis, H. *J. Solid State Chem.* **2001**, *162*, 79.
(31) Goldschmidt, V. M. *J. Chem. Soc.* **1937**, 655.
(32) Shannon, R. D.; Prewitt, C. T. *Acta Crystallogr.* **1969**, *B25*, 925–946.
(33) Shannon, R. D. *Acta Crystallogr.* **1976**, *A32*, 751–767.

conductivity and thermopower was cut from the pressed pellet using a precision wire saw (South Bay Technology). The specimen was polished to a mirror-like finish with SiC sandpaper, using an Ecomet 3000 polisher/grinder from Buehler, washed with ethanol, and dried with acetone to remove remaining particles from the surface before measurements.

Powder X-ray Diffraction (PXRD). X-ray diffraction patterns of the finely ground powder of $Fe_{0.75}Pb_{3.25}Sb_4Se_{10}$ and $FePb_3Sb_4Se_{10}$ were recorded using curved graphite crystal monochromatized Cu Kα radiation (λ = 1.540 56 Å) in reflection geometry on a PANalytical X'pert Pro X-ray powder diffractometer equipped with a position sensitive scintillation counter and operating at 45 kV and 40 mA. To assess the phase purity of $Fe_{0.75}Pb_{3.25}Sb_4Se_{10}$ and $FePb_3Sb_4Se_{10}$, experimental X-ray diffraction patterns were compared to the theoretical patterns simulated using single crystal structure data.

Single Crystal Structure Refinement. Black needle shaped single crystals of $Fe_{0.75}Pb_3Sb_4Se_{10}$ and $FePb_3Sb_4Se_{10}$ with approximate dimensions of 0.016 × 0.06 × 0.22 mm^3 and 0.02 × 0.05 × 0.20 mm^3, respectively, were used for X-ray data collection. The intensity data were recorded at 300 K on a Bruker SMART diffractometer with a CCD detector using a graphite-monochromatized Mo Kα radiation (λ = 0.710 73 Å). The structures were solved and refined using the SHELTXL package.[34]

$FePb_3Sb_4Se_{10}$. Intensity data for $FePb_3Sb_4Se_{10}$ were first indexed in the orthorhombic primitive crystal system with unit cell parameters a = 24.361(2) Å; b = 4.1153(2) Å, c = 19.6918(9) Å, which is consistent with the unit cell parameters of the parent compound $Pb_4Sb_4Se_{10}$ (*Pnma*). Attempts to refine the structure of $FePb_3Sb_4Se_{10}$ in the orthorhombic space group *Pnma* using the atomic positions of $Pb_4Sb_4Se_{10}$ as a starting model resulted in systematic absence violations and a rejection of over half of the collected reflections. This suggested a reduction of the symmetry of the crystal upon substitution of Pb by the smaller Fe atoms. Intensity data were ultimately indexed in the monoclinic crystal system with $\beta \approx 90°$, and the structure was successfully solved by direct methods in the *Pnma* subgroup, $P2_1/m$ (#11) and refined by full-matrix least-squares techniques. The structure solution revealed 16 metal positions and 20 selenium atoms positions. At first, an ordered model based on the atom connectivity in the structure of $Pb_4Sb_4Se_{10}$ was considered. All Pb atoms (Pb(1) to Pb(6)) were located at the 8-fold and 6-fold positions forming the corrugated layer. All Sb atoms (Sb(1) to Sb(8)) were located at the octahedral positions building the NaCl-type ribbon, and Fe atoms (Fe(1) and Fe(2)) were located on the octahedral positions filling the voids between the corrugated layers and the NaCl-type ribbons. The refinement of this model yielded $R_1 \approx 8\%$ with reasonable thermal parameters for all atoms except Fe(1) and Fe(2) which showed slightly smaller thermal parameters indicating mixed site occupancies with a heavier element. Pb(5) and Pb(6) also showed slightly larger thermal parameters than the other Pb atoms. Refinement of Pb/Fe mixed site occupancy on the Fe(1), Fe(2), Pb(5), and Pb(6) positions yielded more acceptable thermal parameters for all atoms with R_1 dropping below 5%. In the final refinement cycles, secondary extinction correction as well as anisotropic displacement parameters for all atoms were included. The occupancy factor of Fe(1) and Fe(2) positions were freely refined to ~75%Fe/25%Pb while Pb(5) and Pb(6) were refined to ~25%Fe/75% Pb. The final composition of the crystal obtained from the refinement was $Fe_{0.96(2)}Pb_{3.04(2)}Sb_4Se_{10}$.

$Fe_{0.75}Pb_{3.25}Sb_4Se_{10}$. Intensity data collected on the $Fe_{0.75}Pb_{3.25}Sb_4Se_{10}$ crystal were indexed in the orthorhombic crystal system with unit cell parameters a = 24.333(5) Å, b = 4.111(1) Å, c = 19.673(4) Å, and the structure was successfully solved by direct methods in the orthorhombic space group *Pnma* (#62) and refined by full-matrix least-squares techniques. The structure solution revealed 8 metal positions and 10 Se positions. Atomic positions were assigned according to the $Pb_4Sb_4Se_{10}$ model, and the refinement strategy was similar to the one described above. Fe/Pb mixed occupancy could be established only on the octahedral positions filling the voids between the corrugated layers and the NaCl-type ribbons. The occupancy factor of the Fe(1) position was freely refined to ~75%Fe/25%Pb, and the final composition of the crystal obtained from the refinement was $Fe_{0.75(2)}Pb_{3.25(2)}Sb_4Se_{10}$. Summary of crystallographic data for both $Fe_{0.75}Pb_{3.25}Sb_4Se_{10}$ and $FePb_3Sb_4Se_{10}$ are given in Table 1. The atomic coordinates and isotropic displacement parameters of all atoms are given as Supporting Information in Table S1. Selected interatomic distances and bonds angles are gathered in Table 2. The software Diamond[35] was utilized to create the graphic representation of the crystal structure with an ellipsoid representation (98% probability level) for all atoms.

Table 1. Selected Crystallographic Data and Details of Structure Determinations for $Fe_{0.75}Pb_{3.25}Sb_4Se_{10}$ (x = 0.75) and $Fe_{0.96}Pb_{3.04}Sb_4Se_{10}$ (x = 0.96)

Formula sum	$Fe_{0.75}Pb_{3.25}Sb_4Se_{10}$ (x = 0.75)	$Fe_{0.96}Pb_{3.04}Sb_4Se_{10}$ (x = 0.96)
Crystal system; space group	Orthorhombic; *Pnma* (#62)	Monoclinic; $P2_1/m$ (#11)
Formula weight (g/mol)	1991.85	1959.7
Density (ρ_{cal}) (g/cm^3)	6.72	6.59
Lattice parameters/Å		
a =	24.333(5) Å	19.6918(9) Å
b =	4.1110(8) Å	4.1153(2) Å
c =	19.673(4) Å	24.3607(11) Å
β =		90.02(1)°
Volume (Å^3); Z	1968(1) Å^3; 4	1974 (2) Å^3; 4
Crystal size (mm^3)	0.016 × 0.06 × 0.22	0.02 × 0.05 × 0.20
Crystal shape, color	Needle-shape, Black	Needle-shape, Black
Radiation/Å	λ(MoK$_\alpha$) = 0.71073	λ(MoK$_\alpha$) = 0.71073
T/K	293	293
μ/cm^{-1}	521	503
Diff. elec. density (e/Å^3)	+1.55 to −1.76	+1.68 to −1.82
$R_1(F_o > 4\sigma(F_o))^a$	0.0293	0.0282
wR_2 (all)^b	0.0717	0.0664
GOF	1.232	1.220

^{a} $R_1 = \sum||F_o| - |F_c||/\sum|F_o|$. ^{b} $wR_2 = [\sum w(F_o^2 - F_c^2)^2/\sum w(F_o^2)^2]^{1/2}$.

Differential Scanning Calorimetry (DSC). Differential scanning calorimetry (DSC) of finely ground powders of $Fe_{0.75}Pb_3Sb_4Se_{10}$ and $FePb_3Sb_4Se_{10}$ was performed to assess melting and crystallization temperatures and the thermal stability of the compounds. DSC data were recorded using approximately 10 mg of finely ground powders of the materials and an equivalent mass of alumina (Al_2O_3) as a reference. Both sample and reference sealed in small quartz tubes under a residual pressure of ~10^{-4} Torr were placed on the sample and reference pans of an F401 DSC apparatus (NETZSCH) maintained under flowing nitrogen gas. The sample and reference were simultaneously heated to 1073 K at a rate of 25 K/min, isothermed for 2 min, and then cooled to 473 K at a rate of 25 K/min. DSC data were recorded during two heating and cooling cycles. The endothermic onset temperature is reported as the melting point, and the exothermic onset temperature is the crystallization point.

Magnetic Property Measurements. Magnetic measurements were performed on polycrystalline samples of $Fe_{0.75}Pb_{3.25}Sb_4Se_{10}$ (~51.4 mg) and $FePb_3Sb_4Se_{10}$ (~125 mg) using a Quantum Design MPMS-XL SQUID magnetometer. DC magnetic susceptibility measurements were performed over a temperature range of 3 to 360 K, and isothermal magnetization measurements were carried out at 2, 300, and 360 K in dc magnetic fields varying from 0 to 10 kOe. In the susceptibility measurements, the samples were first cooled to 3 K under zero magnetic field (ZFC) and the measure-

(34) Sheldrick, G. M. *SHELXTL DOS/Windows/NT Version 6.12*; Bruker Analytical X-ray Instruments, Inc.: Madison, WI, 2000.

(35) Branderburg, K. *DIAMOND. Version 3.1a*; Crystal Impact GbR: Bonn, Germany, 2005.

Table 2. Selected Inter-Atomic Distances (Å) in $Fe_xPb_{4-x}Sb_4Se_{10}$ ($x = 0.75$ and 0.96)[a]

$Fe_{0.75}Pb_{3.25}Sb_4Se_{10}$ ($x = 0.75$)[b]		$Fe_{0.96}Pb_{3.06}Sb_4Se_{10}$ ($x = 0.96$)[c]				$Pb_4Sb_4Se_{10}$ ($x = 0$)[d]	
Pb1−Se2	3.023(9)	Pb1−Se3	3.009(7)	Pb2−Se4	3.013(7)	Pb3−Se3	2.988
Pb1−Se(6,6^{i})	3.038(6)	Pb1−Se(11,11^{i})	3.031(5)	Pb2−Se(12,12^{i})	3.026(5)	Pb3−Se7(×2)	3.096
Pb1−Se(1,1^{i})	3.089(7)	Pb1−Se(1,1^{i})	3.100(6)	Pb2−Se(2,2^{i})	3.105(6)	Pb3−Se6(×2)	3.101
Pb1−Se5^{ii}	3.492(8)	Pb1−Se10^{ii}	3.526(7)	Pb2−Se(15^{ii},15^{iii})	3.524(6)	Pb3−Se1(×2)	3.513
Pb1−Se(8^{ii}, 8^{iii})	3.520(6)	Pb1−Se(16^{ii},16^{iii})	3.528(6)	Pb2−Se9^{ii}	3.527(7)	Pb3−Se10	3.557
Pb2−Se(1,1^{i})	3.112(6)	Pb3−Se(1,1^{i})	3.098(5)	Pb4−Se(2,2^{i})	3.094(6)	Pb2−Se7(×2)	3.109
Pb2−Se(3,3^{i})	3.149(6)	Pb3−Se(5,5^{i})	3.163(5)	Pb4−Se(6,6^{i})	3.161(5)	Pb2−Se8(×2)	3.144
Pb2−Se4	3.192(9)	Pb3−Se7	3.198(7)	Pb4−Se8^{iv}	3.199(7)	Pb2−Se2	3.163
Pb2−Se(7^{iv},7^{v})	3.252(7)	Pb3−Se(14,14^{i})	3.238(6)	Pb4−Se(13,13^{i})	3.237(6)	Pb2−Se5(×2)	3.308
Pb2−Se5^{ii}	3.337(8)	Pb3−Se10^{ii}	3.319(7)	Pb4−Se9^{ii}	3.321(7)	Pb2−Se10	3.312
Pb3−Se10	2.926(10)	Pb5|Fe1−Se19	2.950(8)	Pb6|Fe2−Se20	2.946(8)	Pb4|Sb2−Se9	2.970
Pb3−Se(7,7^{i})	2.942(7)	Pb5|Fe1−Se(13,13^{i})	2.957(6)	Pb6|Fe2−Se(14,14^{i})	2.957(6)	Pb4|Sb2−Se5(×2)	2.976
Pb3−Se(6,6^{i})	3.055(6)	Pb5|Fe1−Se(11,11^{i})	3.059(5)	Pb6|Fe2−Se(12^{v},12^{vi})	3.060(5)	Pb4|Sb2−Se6(×2)	3.028
Pb3−Se9	3.133(9)	Pb5|Fe1−Se17	3.107(7)	Pb6|Fe2−Se18	3.112(7)	Pb4|Sb2−Se4	3.018
Fe1|Pb4−Se10^{v}	2.674(12)	Fe3|Pb7−Se20^{vii}	2.711(7)	Fe4|Pb8−Se19^{ix}	2.707(9)	Pb1|Sb1−Se9	2.969
Fe1|Pb4−Se(10^{ix},10^{x})	2.696(9)	Fe3|Pb7−Se(20,20^{viii})	2.711(7)	Fe4|Pb8−Se(19^{ii},19^{iii})	2.719(7)	Pb1|Sb1−Se9(×2)	2.793
Fe1|Pb4−Se8	2.919(11)	Fe3|Pb7−Se15	2.893(10)	Fe4|Pb8−Se16	2.894(10)	Pb1|Sb1−Se1	2.892
Fe1|Pb4−Se(3,3^{i})	2.924(7)	Fe3|Pb7−Se(5,5^{i})	2.927(6)	Fe4|Pb8−Se(6^{x},6^{ix})	2.922(6)	Pb1|Sb1−Se8(×2)	3.028
Sb1−Se3	2.646(8)	Sb1−Se5	2.650(8)	Sb2−Se6^{ix}	2.660(8)	Sb6|Pb8−Se8	2.691
Sb1−Se(8,8^{vi})	2.758(6)	Sb1−Se(15,15^{xii})	2.784(5)	Sb2−Se(16,16^{xii})	2.776(5)	Sb6|Pb8−Se1(×2)	2.839
Sb1−Se(4,4^{vi})	3.038(7)	Sb1−Se(7,7^{xii})	3.020(6)	Sb2−Se(8,8^{xii})	3.025(6)	Sb6|Pb8−Se2(×2)	3.012
Sb1−Se5	3.159(10)	Sb1−Se9	3.159(8)	Sb2−Se10	3.163(8)	Sb6|Pb8−Se8	3.119
Sb2−Se6	2.674(9)	Sb3−Se11	2.682(8)	Sb4−Se12^{vi}	2.681(8)	Sb4|Pb6−Se6	2.710
Sb2−Se(9,9^{vi})	2.830(8)	Sb3−Se(17,17^{xii})	2.832(6)	Sb4−Se(18,18^{xii})	2.837(6)	Sb4|Pb6−Se4(×2)	2.883
Sb2−Se(2,2^{vi})	3.104(7)	Sb3−Se(3,3^{xii})	3.123(6)	Sb4−Se(4^{vi},4^{xiii})	3.122(6)	Sb4|Pb6−Se3(×2)	3.129
Sb2−Se2^{vii}	3.467(10)	Sb3−Se3^{ii}	3.469(8)	Sb4−Se4^{xiv}	3.471(8)	Sb4|Pb6−Se3	3.509
Sb3−Se1	2.640(9)	Sb5−Se1	2.635(8)	Sb6−Se2	2.640(8)	Sb5|Pb7−Se7	2.675
Sb3−Se(4,4^{vi})	2.878(7)	Sb5−Se(7,7^{xii})	2.887(6)	Sb6−Se(8^{iv},8^{xv})	2.881(6)	Sb5|Pb7−Se3(×2)	2.910
Sb3−Se(2,2^{vi})	2.915(7)	Sb5−Se(3,3^{xii})	2.908(6)	Sb6−Se(4,4^{xii})	2.907(6)	Sb5|Pb7−Se2(×2)	2.924
Sb3−Se9^{vii}	3.324(9)	Sb5−Se17^{ii}	3.333(8)	Sb6−Se18^{xiv}	3.330(8)	Sb5|Pb7−Se4	3.321
Sb4−Se7^{vii}	2.618(9)	Sb7−Se13^{ii}	2.618(8)	Sb8−Se14^{ii}	2.615(8)	Sb3|Pb5−Se5	2.656
Sb4−Se(5,5^{i})	2.738(7)	Sb7−Se(9,9^{i})	2.724(5)	Sb8−Se(10,10^{i})	2.721(6)	Sb3|Pb5−Se10(×2)	2.750
Sb4−Se(9^{vii},9^{viii})	3.206(8)	Sb7−Se(17^{ii},17^{iii})	3.214(6)	Sb8−Se(18^{ii},18^{iii})	3.210(6)	Sb3|Pb5−Se4(×2)	3.237
Sb4−Se4	3.384(9)	Sb7−Se7	3.401(7)	Sb8−Se8	3.401(7)	Sb3|Pb5−Se2	3.415

[a] Standard deviations corresponding to the last digits are indicated in brackets. Corresponding bond distances in the $Pb_4Sb_4Se_{10}$ ($x = 0$) *aristotype* structure are also included for comparison. [b] Operators for generating equivalent atoms for $Fe_{0.75}Pb_{3.25}Sb_4Se_{10}$ ($x = 0.75$): (i) $x, -1 + y, z$; (ii) $0.5 - x, 1 - y, -0.5 + z$; (iii) $0.5 - x, -y, -0.5 + z$; (iv) $-0.5 + x, -1 + y, 0.5 - z$; (v) $-0.5 + x, y, 0.5 - z$; (vi) $x, 1 + y, z$; (vii) $1 - x, 1 - y, 1 - z$; (viii) $1 - x, -y, 1 - z$; (ix) $0.5 - x, -y, 0.5 + z$; (x) $0.5 - x, 1 - y, 0.5 + z$. [c] Operators for generating equivalent atoms for $Fe_{0.96}Pb_{3.06}Sb_4Se_{10}$ ($x = 0.96$): (i) $x, -1 + y, z$; (ii) $1 - x, 1 - y, 1 - z$; (iii) $1 - x, -y, 1 - z$; (iv) $-1 + x, y, z$; (v) $x, -1 + y, -1 + z$; (vi) $x, y, -1 + z$; (vii) $1 - x, -y, -z$; (viii) $1 - x, 1 - y, -z$; (ix) $1 + x, y, z$; (x) $1 + x, -1 + y, z$; (xi) $2 - x, -y, 1 - z$; (xii) $x, 1 + y, z$; (xiii) $x, 1 + y, -1 + z$; (xiv) $-x, 1 - y, 1 - z$; (xv) $-1 + x, 1 + y, z$. [d] Adapted from ref 15.

ments were performed on heating. For the field cooled (FC) measurements, a 100 Oe magnetic field was applied upon cooling to 3 K.

Charge Transport Measurements. Thermopower and electrical conductivity data for $FePb_3Sb_4Se_{10}$ were measured simultaneously using a commercial ZEM-3 Seebeck coefficient/electrical resistivity measurement system (ULVAC-RIKO, Japan). Data were recorded in the temperature range 300 to 570 K. A rectangular shaped specimen with dimensions 2.4 mm × 2.6 mm × 11 mm cut from a 95% dense hot pressed pellet of $FePb_3Sb_4Se_{10}$ was sandwiched between two nickel-based electrodes (current injection) with two voltage probes in perpendicular mechanical contact with the flat and smoothly polished face of the specimen. The specimen, mounted on the sample holder, was then inserted into the furnace chamber, and the system was flushed several times using He gas. The measurement was performed under a residual pressure of He gas (~150 Torr) to facilitate homogeneous distribution of heat inside the furnace chamber. Data were collected on three heating and cooling cycles to ensure reproducibility.

Results and Discussion

Synthesis, X-ray Powder Diffraction, and Thermal Analysis. Single phases of $Fe_{0.75}Pb_{3.25}Sb_4Se_{10}$ and $FePb_3Sb_4Se_{10}$ were successfully synthesized by direct combination of the elements at 823 K. Annealing the reaction mixture at 823 K for 3 days is typically enough to achieve a single phase of $Fe_xPb_{4-x}Sb_4Se_{10}$. However, the crystallinity of the resulting polycrystalline powder is very poor under these conditions and longer annealing times (up to 10 days) are necessary to bring the reaction product into thermodynamic stability. Needle shaped single crystals with a typical size of 0.02 × 0.05 × 0.2 mm^3 are generally grown at the sample location during the long annealing process. A similar synthetic strategy using FeSe instead of elemental Fe as a

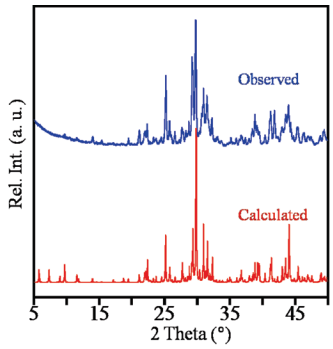

Figure 1. Powder X-ray diffraction pattern of $FePb_3Sb_4Se_{10}$ compared with the theoretical pattern calculated from structure refinement of $Fe_{0.96}Pb_{3.04}Sb_4Se_{10}$.

starting material also resulted in single phases of $Fe_xPb_{4-x}Sb_4Se_{10}$. Attempts to speed the reaction process by increasing the reaction temperature to 973 or 1173 K result in the formation of $Fe_xPb_{4-x}Sb_4Se_{10}$ compounds together with ~10 to 20% Sb_2Se_3 as a minority phase. $Fe_xPb_{4-x}Sb_4Se_{10}$ phases seem to be air stable for several months. However, their thermal stability as revealed by differential scanning calorimetry (DSC) is not very high. $FePb_3Sb_4Se_{10}$ melts congruently at ~873 K and recrystallizes at ~860 K together with impurity phases (Figure S1). This poor stability of $FePb_3Sb_4Se_{10}$ at high temperatures may be the reason why a single phase of the compound could not be achieved by slow cooling of the melt from high temperatures. The formation of $FePb_3Sb_4Se_{10}$ at 823 K instead proceeds by a slow solid-state diffusion process of molten Pb and Se into the solid mass of the reaction mixture. X-ray diffraction on polycrystalline powders of the resulting products (Figure 1) showed an excellent match with the theoretical pattern simulated from the single crystal structure refinement indicating the formation of $FePb_3Sb_4Se_{10}$ as a single phase.

Structure. Despite the fact that bivalent Pb^{2+} and Fe^{2+} ions both prefer a 6-fold coordination environment when combined with chalcogenides, the idea of partial or full substitution of Pb by Fe into ternary heavy main group metal chalcogenides seems to be unreasonable. According to the Goldschmidt rule, atomic substitution within a structure is primarily controlled by (1) the radii and (2) the charge of the ions substituting each other. Free substitution will occur for the difference between effective ionic radii $\Delta R \leq 15\%$. For $15\% \leq \Delta R \leq 30\%$, limited substitution is possible. If $\Delta R > 30\%$, there will be little to no substitution.[31] Considering the effective ionic radii of Pb^{2+} (1.19 Å) and Fe^{2+} (low spin, 0.61 Å; high spin, 0.78 Å) for a 6-fold coordination,[32,33] the large difference ($\Delta R \approx 34\%$ (HS) and 49% (LS)) strongly points to almost impossible substitution between both elements. However, under special conditions where, for example, the size of the targeted octahedral polyhedron can be significantly altered by structural distortions (expansion or contraction of the unit cell), both elements can isomorphically substitute each other. In such circumstances, Fe^{2+} ions will likely adopt the high spin (HS) state, as the deviation from the effective ionic radius of Pb will be smaller (~34%) than if Fe^{2+} ions were in a low spin (LS) state (~49%). This geometrical flexibility requirement seems to be very well satisfied in the structure of the $Pb_4Sb_4Se_{10}$ phase. As depicted in Figure 2, the 3D network formed by the corrugated layers (bicapped trigonal prisms and octahedra around Pb atoms) and the NaCl-type ribbons of edge-sharing $\{SbSe_6\}$ octahedra provide voids that are large enough to accommodate a double-chain of edge-sharing octahedra. The

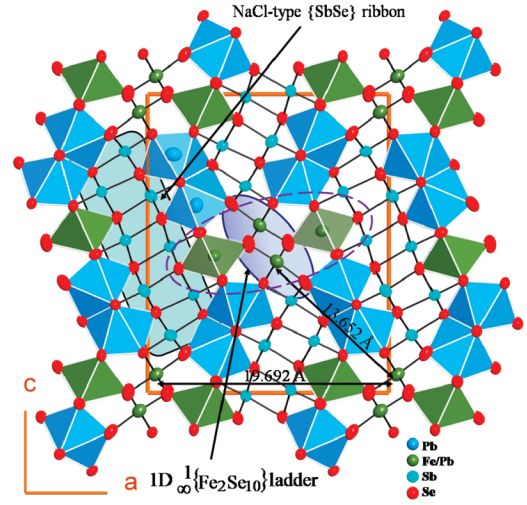

Figure 2. Crystal structure of $Fe_xPb_{4-x}Sb_4Se_{10}$ ($x = 0.96$) projected along [010]. The corrugated layers, {SbSe} ribbons, and the quasi 1D $\{M_2Se_{10}\}$ ladder (blue ellipsoid) and $\{MSe_6\}-\{M_2Se_{10}\}-\{MSe_6\}$ tetrameric chain (purple dashed ellipsoid) are highlighted. The intrachain and interchain separations between magnetic centers in the structure of $Fe_{0.96}Pb_{3.04}Sb_4Se_{10}$ are provided.

open spaces around the double chain provide flexibility for the octahedra to expand or contract as necessary to accommodate changes in the nature of the "guest" atom (Fe or Pb in this case). As can be observed from the change in the lattice parameters of $Fe_{0.75}Pb_{3.25}Sb_4Se_{10}$ ($a = 24.3330(5)$ Å, $b = 4.1110(8)$ Å, $c = 19.673(4)$ Å) obtained from single crystal refinement (Table 1), the partial substitution of Pb by Fe within the double chain in the structure of the parent compound $Pb_4Sb_4Se_{10}$ ($a = 24.591(8)$ Å, $b = 19.757(8)$ Å, $c = 4.166(8)$ Å) results in a notable contraction of the unit cell volume (~3%) while maintaining the overall symmetry of the original structure. The refinement of the structure of $Fe_{0.75}Pb_{3.25}Sb_4Se_{10}$ indicated that Fe atoms are exclusively located within the double chain (we will refer to this as the Fe-ladder) with approximately 75% of Pb atoms replaced by Fe. Consequently, the shape of the coordination polyhedron changes from the [2 + 4] distortion to a more regular [3 + 3] octahedral configuration. Bond distances between the central atom (Fe/Pb) and the Se atoms of the coordination sphere are not equally affected by the substitution. The most severe contraction of ~9% is observed between the central atom and the Se(10) atom connecting the Fe-ladder to the corrugated layer (Table 2). This particular bond contracts from 2.969 Å in $Pb_4Sb_4Se_{10}$ to 2.674(2) Å in $Fe_{0.75}Pb_{3.25}Sb_4Se_{10}$. Interestingly, when more Pb atoms in the structure of $Pb_4Sb_4Se_{10}$ are substituted by Fe atoms as is the case in $Fe_{0.96}Pb_{3.04}Sb_4Se_{10}$, the unit cell volume does not continue to contract as would normally be expected. Instead, a slight expansion of the cell parameters ($a = 19.6918(9)$ Å, $b = 4.1153(2)$ Å, $c = 24.361(2)$ Å; $\beta = 90.02°$) with reduction of the symmetry of the overall structure from orthorhombic to monoclinic was observed. Reasonable explanations of this *apparently* abnormal expansion of the unit cell upon increasing the Fe content as well as the reduction in the crystal symmetry from orthorhombic to monoclinic are provided below.

In addition to the abnormal change in the unit cell parameters, the refinement of the structure of $Fe_{0.96}Pb_{3.04}Sb_4Se_{10}$ also indicated that the increase in the proportion of Fe atoms in the structure of $Pb_4Sb_4Se_{10}$ does not translate into an increase in the fraction of Fe substituting Pb within the double chain (Fe-ladder) as would be expected. The amount of Fe substituting

Pb within the Fe-ladder remains unchanged (~75%) while the "excess" of Fe atoms (~ 25%) instead substitute Pb atoms at the octahedral position located within the corrugated layers (Table S1). It is still unclear what maximum amount of Fe can potentially be inserted in the octahedral Pb positions within the Fe-ladder before triggering the substitution in the octahedral position within the corrugated layer. However, the fact that both structures contain nearly 75% Fe in the Fe-ladder suggests that this critical occupation may be close to 75%. The absolute determination of this fraction could provide valuable information about the approximate composition at which the transition from orthorhombic to monoclinic symmetry occurs. Also, questions of the substitution limit of Pb by Fe in the structure of $Pb_4Sb_4Se_{10}$ including that of the existence of the hypothetical composition $Fe_2Pb_2Sb_4Se_{10}$ in which both octahedral positions would be completely filled by Fe atoms are still unanswered. These studies are currently in progress and will be reported later. The observed atomic distribution in the structure of $Fe_{0.96}Pb_{3.04}Sb_4Se_{10}$ gives rise to the formation of isolated "clusters" of four octahedra (tetramers) sharing corners and edges to build quasi-one-dimensional chains running parallel to the *b*-axis. This clustering of Fe atoms induces a slight expansion of bond distances in both octahedral positions as can be appreciated from the comparison of corresponding bonds in Table 2. It is important to note that the substitution of Pb by Fe in the structure of $Pb_4Sb_4Se_{10}$ does not involve the Pb atom located at the 8-fold coordinated position within the corrugated layer. A likely reason for this site discrimination is that the volume of the bicapped trigonal prisms is too large for the small Fe atoms.

Structure−Composition and Group−Subgroup Relationships. The structures of $Fe_xPb_{4-x}Sb_4Se_{10}$ ($x = 0.75$ and 0.96) are both *derivatives* of the $Pb_4Sb_4Se_{10}$ structure type where partial substitution of Pb atoms in octahedral positions retained the overall topology of the original structure (*aristotype*). Upon increasing the Fe content, the resulting quaternary composition with $0 \le x \le 0.75$ maintained the orthorhombic symmetry of the $Pb_4Sb_4Se_{10}$ parent structure. As observed from the structure refinement of the composition ($x = 0.75$), Fe atoms in this case are exclusively located in octahedral positions within the $\{M_2Se_{10}\}$ (ladder) dimeric chain (Figure 3A and 3B). The replacement of Pb by Fe atoms is followed by a small contraction of the unit cell as would be expected from the difference in the effective ionic radii of both elements.[32,33] The situation where Fe content approaches $x = 1$ is particularly interesting as there is a competing distribution of Fe atoms between octahedral positions within the $\{M_2Se_{10}\}$ ladder and the octahedral positions forming the $\{MSe_6\}$ single chain (Figure 3C) within the corrugated layer. In the ideal situation, Fe atoms would fully substitute Pb atoms within the $\{M_2Se_{10}\}$ ladder resulting in an ordered structure. In this case the orthorhombic symmetry might be maintained. Alternatively, Fe can partially substitute Pb atoms in both octahedral positions giving rise to "clusters" of corner-sharing $\{M_2Se_{10}\}$ (ladders) and $\{MSe_6\}$ single chains (Figure 3A). The latter situation was observed from the structure refinement of the composition $x = 0.96$, where ~75% of Fe atoms are located within the $\{M_2Se_{10}\}$ ladder and ~25% partially substitute Pb atoms in the $\{MSe_6\}$ single chain. This structural arrangement results in a phase transition which is accompanied by a reduction of the overall symmetry of the crystal from the orthorhombic space group *Pnma* (#62) to the maximal nonisomorphic subgroup $P2_1/m$ (#11). The monoclinic angle β is close to 90° suggesting that the composition with $x \approx 1$ is near the borderline of the phase transition from the orthorhombic to the monoclinic structure. The group−subgroup relationship between the two structures is depicted in Figure 4. The direct crystallographic consequence of the reduction in symmetry is the splitting of each atomic position (Wyckoff position: 4*c*) of the orthorhombic unit cell into two independent atomic positions (Wyckoff position: 2*e*). Atomic coordinates in the monoclinic structure are related to those of the orthorhombic structure. In the orthorhombic structure, each atomic position with general coordinate (x, y, z) splits into two independent positions with atomic coordinates (x, y, z) and ($0.5 - x$, y, $0.5 + z$) in the monoclinic structure.

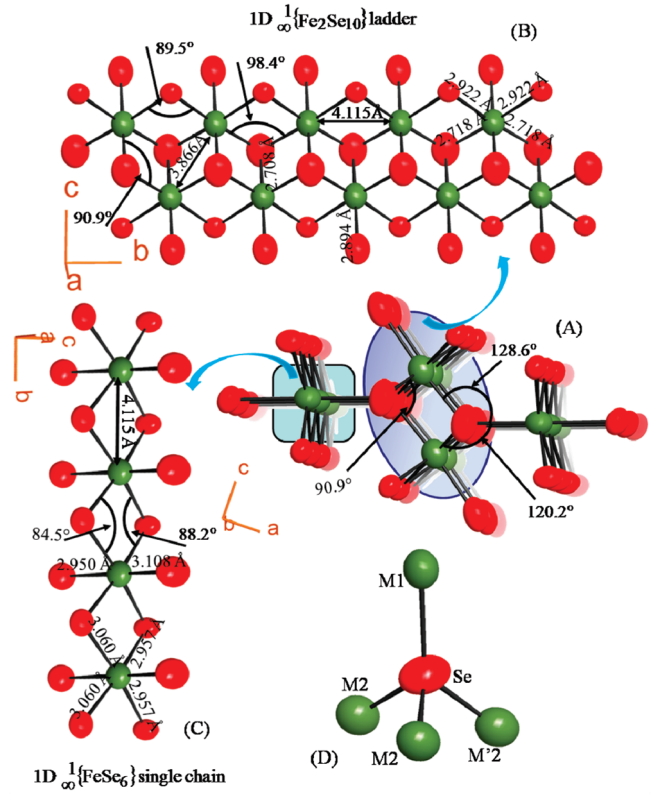

Figure 3. Geometric details of the magnetic substructure in $Fe_xPb_{4-x}Sb_4Se_{10}$. Bond distances and angles corresponds to the composition $x = 0.96$. (A) 1D $\{MSe_6\}-\{M_2Se_{10}\}-\{MSe_6\}$ tetrameric chain; (B) 1D $\{M_2Se_{10}\}$ ladder; (C) 1D $\{MSe_6\}$ single chain; and (D) coordination of the Se atom bridging $\{MSe_6\}$ and $\{M_2Se_{10}\}$ chains. Bond distances and angles within the tetrahedral coordination around the bridging Se atom in the structures of $Fe_xPb_{4-x}Sb_4Se_{10}$ ($x = 0$, 0.75, and 0.96) are compared in Table 3.

Another interesting consequence of the transition from the orthorhombic to the monoclinic structure near composition $x = 1$ is the anomalous expansion of the unit cell. The cell volume (measured at 300 K) increases from 1967.95(69) Å^3 for $x = 0.75$ to 1974.13(16) Å^3 for $x = 0.96$, which results in a notable reduction of the theoretical density of the crystal from 6.72 g/cm^3 for $Fe_{0.75}Pb_{3.25}Sb_4Se_{10}$ to 6.59 g/cm^3 for $Fe_{0.96}Pb_{3.04}Sb_4Se_{10}$. This observation is in opposition to the expected cell contraction upon increased removal of large Pb atoms and substitution with small Fe atoms. A reasonable explanation of this behavior can be derived from a comparison of the geometrical parameters of the tetrahedral coordination of the Se atom bridging the $\{M_2Se_{10}\}$ and $\{MSe_6\}$ chains (Figure 3D) in the structures $Pb_4Sb_4Se_{10}$ ($x = 0$), $Fe_{0.75}Pb_{3.25}Sb_4Se_{10}$ ($x = 0.75$), and $Fe_{0.96}Pb_{3.04}Sb_4Se_{10}$ ($x = 0.96$) (Table 3). As depicted in Figure 3B, the $\{M_2Se_{10}\}$ ladder and the $\{MSe_6\}$ single chains share corners to form an irregular tetrahedron around the shared Se

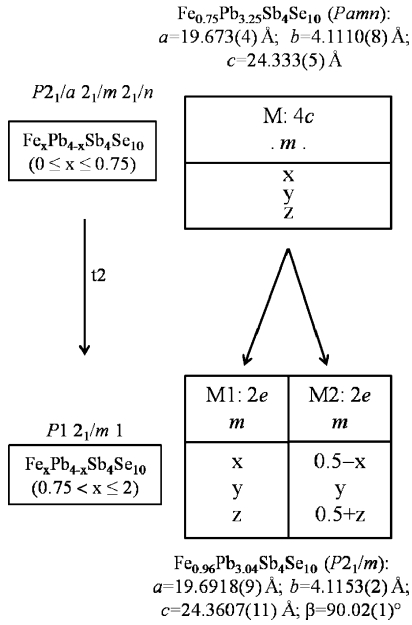

Figure 4. Group−subgroup relationship between the orthorhombic and the monoclinic structures of $Fe_xPb_{4-x}Sb_4Se_{10}$ (x = 0.75 and 0.96). To simplify the relationship between atomic coordinates in both structures, the original setting *Pnma* was converted to the *Pamn* space group by permutation of a and c axis.

Table 3. Comparison of Bond Lengths and Angles within the Tetrahedral Coordination of the Se Atom Bridging $\{M_2Se_{10}\}$ Dimeric and $\{MSe_6\}$ Single Chains in the Structures of $Fe_xPb_{4-x}Sb_4Se_{10}$ (x = 0.0, 0.75, and 0.96)

Geometric parameters	x = 0 (M1 = M2 = Pb)	x = 0.75 (M1 = Pb; M2 = Fe/Pb)	x = 0.96 (M1 = Pb/Fe; M2 = Fe/Pb)
M1−Se (d1)	2.970 Å	2.927(1) Å	2.946(1) Å
M2−Se (d2)	2.793 Å	2.696 (1) Å	2.710(1) Å
M′2−Se (d3)	2.969 Å	2.674(1) Å	2.715(1) Å
M1−Se−M2	122.1°	119.7°	120.2°
M1−Se−M′2	127.1°	129.1°	128.6°
M2−Se−M′2	90.1°	90.6°	90.6°

atom. The M1−Se (d1) bond distance between the shared Se atom and the metal atom within the $\{MSe_6\}$ single chain is 2.970 Å in $Pb_4Sb_4Se_{10}$ (x = 0) (Table 3). The distance decreases slightly to 2.927(2) Å in $Fe_{0.75}Pb_{3.25}Sb_4Se_{10}$ (x = 0.75) upon partial substitution of Pb by Fe within the $\{M_2Se_{10}\}$ ladder. The corresponding bond distance surprisingly increases to 2.946 Å in $Fe_{0.96}Pb_{3.04}Sb_4Se_{10}$ (x = 0.96) when Fe substitutes Pb in both octahedral positions. The bond distances between the shared Se atom and the metal atoms within the $\{M_2Se_{10}\}$ ladder appear to be more sensitive to the substitution of Pb by Fe atoms. The M2−Se (d2 and d3) bond distances in $Pb_4Sb_4Se_{10}$ (x = 0) are 2.793 and 2.969 Å, respectively. The corresponding bond lengths decrease to 2.696 and 2.674 Å in $Fe_{0.75}Pb_{3.25}Sb_4Se_{10}$ (x = 0.75) upon partial substitution of Pb by Fe within the $\{M_2Se_{10}\}$ ladder. In $Fe_{0.96}Pb_{3.04}Sb_4Se_{10}$ (x = 0.96), the corresponding bond distances increase to 2.710 and 2.715 Å as Fe is substituting Pb in both octahedral positions. Similar trends can be observed in M1−Se−M2, M1−Se−M′2, and M2−Se−M′2 bond angles (Table 3). From the above analysis, it appears that the abnormal change in the geometric parameters is observed only when the smaller Fe atom substitutes Pb in both single and dimeric (ladder) chains. The observed atomic distribution might normally be expected only for compositions with $x > 1$ after all Pb atoms within the $\{M_2Se_{10}\}$ ladder have been replaced by Fe. Theoretically, full substitution of Pb by Fe within the $\{M_2Se_{10}\}$ ladder should lead to severe shrinking of the octahedral coordination due to large size mismatch (34%) between both elements. The reduction in the size of the octahedra within the $\{M_2Se_{10}\}$ ladder, in addition to the repulsive forces resulting from the interaction of Fe atoms in the edge-sharing octahedral environments, would cause tremendous stress on the robust three-dimensional framework structure (built by the corrugated layers and the NaCl-type ribbons). The stress is prevented by a symmetry breaking transition from the orthorhombic to the monoclinic structure and a distribution of Fe atoms into both the $\{M_2Se_{10}\}$ ladder and the $\{MSe_6\}$ single chain.

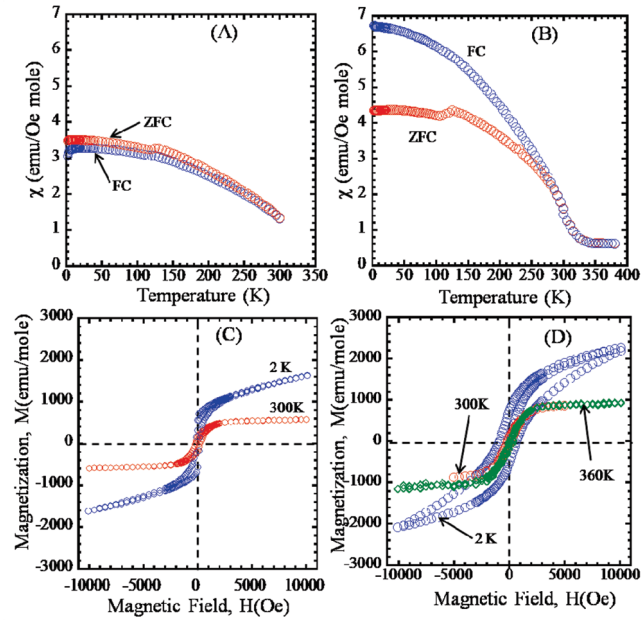

Figure 5. Above: Temperature dependent magnetic susceptibilities of (A) $Fe_{0.75}Pb_{3.25}Sb_4Se_{10}$ (x = 0.75) and (B) $FePb_3Sb_4Se_{10}$ (x = 1) measured in an applied magnetic field of 100 Oe. Red and blue symbols are field cooled (FC) and zero field cooled (ZFC) data respectively. Below: Field dependent magnetization of (C) $Fe_{0.75}Pb_{3.25}Sb_4Se_{10}$ (x = 0.75) and (D) $FePb_3Sb_4Se_{10}$ (x = 1) measured at 2, 300, and 360 K with applied fields of up to 10 kOe.

Magnetism. The observed distribution of Fe atoms within the structures of $Fe_{0.75}Pb_{3.25}Sb_4Se_{10}$ and $Fe_{0.96}Pb_{3.04}Sb_4Se_{10}$ can be generalized by the formula $Fe_xPb_{4-x}Sb_4Se_{10}$ where $0 \le x \le 2$. It is expected that all members of the $Fe_xPb_{4-x}Sb_4Se_{10}$ family of compounds ($0 < x \le 2$) will exhibit some degree of magnetism given the presence of the transition metal Fe^{2+} cation and its d^6 electronic configuration. Temperature dependent magnetic susceptibility (field cooled and zero field cooled) measured in an applied field of 100 Oe for $Fe_{0.75}Pb_{3.25}Sb_4Se_{10}$ (x = 0.75) and $FePb_3Sb_4Se_{10}$ (x = 1) compositions showed that the compounds are ferromagnetic below 300 K and exhibit superparamagnetism at higher temperatures (Figure 5A and 5B). For the sample with x = 1, there is a sharp divergence between the field-cooled (FC) and the zero-field-cooled (ZFC) data below the blocking temperature of ~280 K. The ZFC susceptibility curve of $FePb_3Sb_4Se_{10}$ shows a fast increase at the transition temperature and a downturn at approximately T = 150 K after which the susceptibility increases slowly with decreasing temperature. Similar behavior was also found on the ZFC data of $Fe_{0.75}Pb_{3.25}Sb_4Se_{10}$ (x = 0.75). The downturn in the susceptibility observed on the ZFC data is weaker on the FC data, and the magnetic susceptibility increases monotonically with decreasing temperature. The observed downturn in the suscep-

tibility could be an indication of spin frustration or spin glass behavior. Upon increasing the Fe content from $x = 0.75$ to $x = 1$, the FC magnetic susceptibility almost doubles (Figure 5A and 5B). The ferromagnetic behavior of $Fe_{0.75}Pb_{3.25}Sb_4Se_{10}$ and $FePb_3Sb_4Se_{10}$ samples was also observed in the isothermal magnetization data (Figure 5C and 5D). Magnetization data at 2 K show a mild hysteresis with a coercive force of ~800 Oe for $x = 1$, typical for a soft ferromagnet. A smaller hysteresis was observed for the composition with $x = 0.75$. At this temperature, the saturation magnetization could not be reached with an applied external field of up to 10 000 Oe. At room temperature, the magnetization curve still showed a small hysteresis with a coercive force of ~160 Oe ($x = 1$). Above room temperature the $FePb_3Sb_4Se_{10}$ ($x = 1$) sample exhibits superparamagnetic behavior with a saturation magnetization value of ~950 emu/mol at an applied field of 4000 Oe. The saturation magnetization for the $Fe_{0.75}Pb_{3.25}Sb_4Se_{10}$ ($x = 0.75$) sample at 300 K is ~600 emu/mol. At low T (2 K), the observed value of magnetization is ~1650 emu/mol for $x = 0.75$ and ~2200 emu/mol for $x = 1$. If we convert these values to magnetic moment per Fe, we find a value of ~0.40 μ_B, which is only 10% of the expected value of 4.0 μ_B if all spins of Fe^{2+} are localized and ordered at low temperature. This dramatic reduction in the moment (within a localized Fe^{2+} moment picture) strongly suggests that the system is not an ordinary ferromagnet where all the magnetic spins are parallel. To understand the magnetic behavior of this family of compounds, we have analyzed the coupling between spins located on adjacent Fe atoms using the Goodenough−Kanamori rules.[23−25]

The nature of magnetic ordering as well as the strength of magnetization in $Fe_xPb_{4-x}Sb_4Se_{10}$ phases can be controlled by the distribution of the Fe atoms within the "cluster" of the edge and corner sharing $\{M_2Se_{10}\}$ ladder and $\{MSe_6\}$ single chain running parallel to the b-axis (Figure 3A). These clusters are magnetically isolated from each other, being separated by the NaCl-type {SbSe} ribbons (Figure 2). The shortest intercluster distance in the structure of $Fe_{0.96}Pb_{3.04}Sb_4Se_{10}$ for example is 13.652 Å. The magnetic properties of the $Fe_xPb_{4-x}Sb_4Se_{10}$ compounds can therefore be understood in light of the intracluster exchange interactions between magnetic ions located inside the $\{M_2Se_{10}\}$ ladder and $\{MSe_6\}$ single chain. At this point, two cases should be considered depending on the value of compositional parameter x.

The first case is when the magnetic element (Fe) in the structure is located only within the one-dimensional $\{M_2Se_{10}\}$ ladder. This situation is observed in the structure of $Fe_{0.75}Pb_{3.25}Sb_4Se_{10}$. Within the $\{M_2Se_{10}\}$ ladder, the magnetic atoms form two parallel rows shifted by $b/2$ (Figure 3B). This arrangement results in isosceles triangles of Fe atoms with metal−metal distances of 3.866 Å between chains and 4.111 Å along an individual chain. The large separations between magnetic atoms preclude all direct magnetic-exchange interactions between the magnetic moments on neighboring Fe atoms. The magnetic atoms interact via indirect exchange interactions through the Se atom bridging two adjacent Fe atoms. According to the Goodenough−Kanamori rules,[23−25] the nature of the magnetic interaction between spins located on adjacent Fe atoms strongly depends on the M−Se−M bond angles. It was predicted that a 180° M−Se−M bond angle gives rise to strong antiferromagnetic (AFM) coupling (due to an overlap of magnetically active orbitals) while a 90° bond angle favors weak ferromagnetic coupling (due to strict orthogonality of the occupied orbitals). As can be seen from Figure 3A, the shared edge

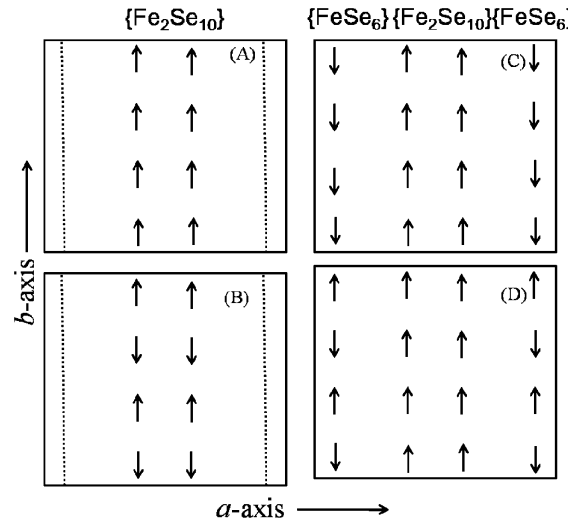

Figure 6. Proposed spin models for $Fe_xPb_{4-x}Sb_4Se_{10}$ family of compounds. (A) and (B) correspond to compositions with $0 < x \leq 0.75$ in which only the $\{M_2Se_{10}\}$ ladder is present. (A) The interchain and intrachain interactions (within the ladder) are both ferromagnetic; (B) the interchain interaction is ferromagnetic whereas the intrachain interaction is antiferromagnetic. For $Fe_xPb_{4-x}Sb_4Se_{10}$ compounds with $x \geq 0.96$, both the $\{MSe_6\}$ single chain and the $\{M_2Se_{10}\}$ ladder are present. The spin models in (C) and (D) assume ferromagnetic coupling within the $\{M_2Se_{10}\}$ ladder. In (C) spins within the $\{MSe_6\}$ single chain are coupled ferromagnetically, while in (D) they are coupled antiferromagnetically.

between octahedra (ac plane) within the $\{M_2Se_{10}\}$ ladder is formed by an equatorial Se atom (that lies on the square plane of the octahedron) and the apical one. This type of geometric arrangement of octahedra (*cis*-type) minimizes interactions between magnetically active orbitals in each MSe_6 octahedron. The connectivity type in addition to the M−Se−M bond angle of ~90.9° indicates that the exchange interaction between spins located on adjacent Fe atoms from both chains of the $\{M_2Se_{10}\}$ ladder should be ferromagnetic. When looking along the b-axis, octahedra within the $\{M_2Se_{10}\}$ ladder share edges formed by two equatorial Se atoms (*trans*-type). Although this geometrical arrangement does not prevent overlap between magnetically active orbitals as much as in the *cis*-type described above, the observed M−Se−M bond angles of 89.5° and 98.4° also suggest weak ferromagnetic or antiferromagnetic coupling of spins located on adjacent Fe atoms in an individual chain. It is possible that in this case an antiferromagnetic exchange between two adjacent spins through direct hopping may also be significant. According to the above analysis, one can have two possible magnetic coupling scenarios. One, the interactions between nearest magnetic atoms belonging to two different chains (inter) of the ladder and those belonging to the same chain (intra) are both ferromagnetic (Figure 6A). Two, the interchain interaction is ferromagnetic whereas the intrachain interaction is antiferromagnetic (Figure 6B). In this case there will be competition between ferro- and antiferromagnetic couplings, and depending on the relative strengths, one can have either a ferromagnetic or a spiral ground state.

The second case is when the magnetic element (Fe) is found simultaneously in both the one-dimensional $\{M_2Se_{10}\}$ ladder and the $\{MSe_6\}$ single chain. This corresponds to the situation observed in the structure of $Fe_{0.96}Pb_{3.04}Sb_4Se_{10}$. In this case, the $\{MSe_6\}$ single chain and the $\{M_2Se_{10}\}$ ladder share corners to form a unique $\{MSe_6\}-\{M_2Se_{10}\}-\{MSe_6\}$ cluster, called "tetramers". The intratetramer magnetic ordering will be influenced by (1) the ferromagnetic (FM) or competing exchange

interaction in the $\{M_2Se_{10}\}$ ladder as described above, (2) the nature of the magnetic coupling in the $\{MSe_6\}$ single chain, and (3) the coupling between both magnetic moments of the ladder and the chain. Detailed analysis of the bond distances and angles within the $\{MSe_6\}$ single chain in the structure of $Fe_{0.96}Pb_{3.04}Sb_4Se_{10}$ (Figure 3C) in light of the Goodenough−Kanamori rules indicates that both antiferromagnetic and ferromagnetic coupling are possible. The indirect magnetic exchange pathway with an M−Se−M bond angle of 88.2° points toward a weak ferromagnetic coupling of spins located on adjacent magnetic atoms while the pathway with a bond angle of 84.5° favors antiferromagnetic coupling. It should be noted that the Se atom bridging the $\{MSe_6\}$ single chain and the $\{M_2Se_{10}\}$ ladder is located in a distorted tetrahedral environment with three metal atoms from the $\{M_2Se_{10}\}$ ladder forming the isosceles triangular base (equatorial) and a metal atom from the $\{MSe_6\}$ single chain at the apical position (Figure 3D). The M−Se−M bond angles between the apical atom and metal atoms on the equatorial base are ∼120° and ∼128° ($x = 0.96$), which strongly suggest antiferromatic coupling between magnetic moments from the $\{MSe_6\}$ single chain and the $\{M_2Se_{10}\}$ ladder. In this situation, the nature and magnitude of the magnetic interaction within the $\{MSe_6\}$ single chain are critical in determining the nature and magnitude of the overall intratetramer magnetic exchange interaction. However, one should note that for Fe concentrations $x \approx 1$ or less, the $\{MSe_6\}$ chains are only 25% occupied by Fe, so that the interaction between spins belonging to the chain may not be relevant to the final observed magnetism in this system. If on the other hand the $\{MSe_6\}$ chains were fully occupied as would happen for larger x values, the type of interaction between these spins will be significant. For example, assuming ferromagnetic coupling within the $\{M_2Se_{10}\}$ ladder, ferromagnetic coupling of spins within the $\{MSe_6\}$ chain (Figure 6C) would result in intratetramer antiferromagnetic exchange interaction (overall magnetic moments from single chains and ladder are of similar magnitude) while antiferromagnetic coupling of spins within the $\{MSe_6\}$ chain (Figure 6D) would result in a weaker intratetramer ferromagnetic exchange interaction (overall magnetic moments from single chains are smaller than the magnetic moment within the ladder). The ability of spins within the $\{MSe_6\}$ single chain to order either ferromagnetically or antiferromagnetically could result in competition between both ordering pathways that may result in multiple ordering transitions or ordering over a broad temperature range.

In light of the above analysis based on a localized Fe^{2+} moment, we can conclude that the magnetism within the ladder and ladder−single chain systems in $Fe_xPb_{4-x}Sb_4Se_{10}$ phases is controlled by competing interactions. If on the other hand one wants to understand the magnetism of these compounds within an itinerant model, one has to carry out local spin density calculations to see if there is a ferromagnetic state and what is the moment/Fe. One should however note that because of the one-dimensionality, one expects to see strong quantum spin fluctuation effects which tend to reduce the moment from the values calculated using local spin density theory. A detailed analysis of these ideas and their impact on the observed magnetic properties are under investigation.

Charge Transport Properties. Figure 7A shows the temperature dependence of the electrical conductivity of $FePb_3Sb_4Se_{10}$ ($x = 1$). The electrical conductivity of $FePb_3Sb_4Se_{10}$ increases monotonically with rising temperature from a room temperature value of ∼0.27 S/cm to ∼1 S/cm at 600 K. The observed

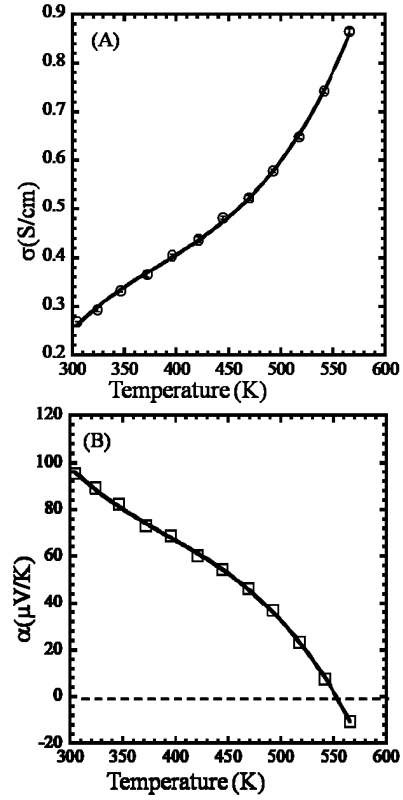

Figure 7. Temperature dependent charge transport properties of $FePb_3Sb_4Se_{10}$. (A) Electrical conductivity; (B) Thermopower.

increase in the electrical conductivity with temperature is in agreement with Arrhenius's law ($\sigma = \sigma_0 \exp(-\Delta E/kT)$, where σ_0 is the electrical conductivity at zero absolute temperature, k is the Boltzmann constant, and ΔE is the activation energy[36] and indicates that $FePb_3Sb_4Se_{10}$ is an intrinsic semiconductor. The plot of the logarithm of the electrical conductivity as a function of inverse temperature results in an activation energy of ∼0.05 eV suggesting poor metallic character for $FePb_3Sb_4Se_{10}$. The rather poor electrical conductivity observed for $FePb_3Sb_4Se_{10}$ is probably due to the low mobility of charge carriers within the conduction band.

$FePb_3Sb_4Se_{10}$ showed positive thermopower values between 300 and 550 K indicating p-type semiconducting behavior (Figure 7B). The thermopower decreases from ∼90 μV/K at 300 K to ∼0 μV/K at 550 K. A further increase in temperature results in the conduction switching to n-type as indicated by the negative values of the thermopower. The decrease in thermopower with rising temperature can be understood by a simple mechanism in which thermally excited electrons from the top of the valence band easily cross to the conduction band, because of the very small energy gap (∼0.05 eV). The negative values of the thermopower above 550 K suggest that charge transport within the conduction band is dominated by thermally excited electrons.

Concluding Remarks

$Fe_xPb_{4-x}Sb_4Se_{10}$ ($0 \le x \le 2$), a new family of quasi-one-dimensional ferromagnetic semiconducting selenides, was generated by isoelectronic substitution of Pb atoms in octahedral positions within the structure of the ternary $Pb_4Sb_4Se_{10}$ com-

(36) Arrhenius, S. *Z. Phys. Chem.* **1889**, *4*, 226.

pound by magnetic Fe atoms. Despite the large difference (~34%) in their effective atomic radii, the substitution between Fe and Pb in $Pb_4Sb_4Se_{10}$ is isomorphic and the resulting $Fe_xPb_{4-x}Sb_4Se_{10}$ quaternary compounds maintain the orthorhombic symmetry of the ternary parent phase for Fe content $x \leq 0.75$. Phase transition to the monoclinic symmetry occurs with larger Fe content ($x > 0.75$). Single phases of two members of the $Fe_xPb_{4-x}Sb_4Se_{10}$ ($0 \leq x \leq 2$) family of compounds with $x = 0.75$ and $x = 1$ were prepared via solid-state reaction of the elements at 823 K. Both phases show ferromagnetic behavior as the result of the substitution of nonmagnetic Pb atoms by the magnetic transition metal element Fe. Their crystal structures contain the rather unusual quasi-one-dimensional $\{Fe_2Se_{10}\}$ ladders of edge-sharing octahedra magnetically isolated by the semiconducting {SbSe} ribbons. For compositions with a large Fe content ($x > 0.75$), the $\{Fe_2Se_{10}\}$ ladders share corners with additional $\{FeSe_6\}$ single chains to form unique tetrameric (cluster) chains of octahedrally coordinated Fe atoms. This unusual clustering of octahedrally coordinated Fe atoms is believed to be responsible for the complex ferromagnetic behavior observed in $Fe_xPb_{4-x}Sb_4Se_{10}$ phases with $x = 0.75$ and $x = 1$. Analysis of the geometrical parameters within the ladders and single chains and the observed dramatic reduction in the moment (within the context of a localized Fe^{2+} moment) of $Fe_{0.75}Pb_{3.25}Sb_4Se_{10}$ and $FePb_3Sb_4Se_{10}$ compounds strongly suggests that the $Fe_xPb_{4-x}Sb_4Se_{10}$ phases are not ordinary ferromagnets where all the magnetic spins are parallel at low temperatures. The magnetism in the ladder and ladder−single chain systems in $Fe_xPb_{4-x}Sb_4Se_{10}$ phases is rather controlled by competing interactions. Additionally, electronic charge transport measurements indicated that $FePb_3Sb_4Se_{10}$ is a narrow-gap p-type semiconductor between 300 and 550 K and switches to n-type conduction above 550 K.

Acknowledgment. This work was partially supported by the National Science Foundation (DMR-0954817), the Louisiana Board of Regents (Grant # NSF(2008)-PFUND-126) and start-up funds from the University of New Orleans Office of Research and Sponsored Programs. The authors thank Prof. S. D. Mahanti (MSU) for helpful discussions, Prof. Edwin Stevens for the use of Smart CCD (Bruker) single crystal diffractometer, and Dr. Hongxue Lui for the magnetic susceptibility measurement on $FePb_3Sb_4Se_{10}$.

Supporting Information Available: X-ray crystallographic data in CIF format for the single crystal refinements of $Fe_{0.75}Pb_{3.25}Sb_4Se_{10}$ ($x = 0.75$) and $Fe_{0.96}Pb_{3.04}Sb_4Se_{10}$ ($x = 0.96$). Table of atomic coordinates, site occupancy factors, and equivalent isotropic displacement parameters for $Fe_{0.75}Pb_{3.25}Sb_4Se_{10}$ ($x = 0.75$) and $Fe_{0.96}Pb_{3.04}Sb_4Se_{10}$ ($x = 0.96$). Differential scanning calorimetry (DSC) curves of $FePb_3Sb_4Se_{10}$. Plots of χ^*T vs T for $Fe_{0.75}Pb_{3.25}Sb_4Se_{10}$ ($x = 0.75$) and $FePb_3Sb_4Se_{10}$ ($x = 1$). This material is available free of charge via the Internet at http://pubs.acs.org.

JA910545E